ELSEVIER

Journal of Volcanology and Geothermal Research 115 (2002) 1–18

Journal of volcanology and geothermal research

www.elsevier.com/locate/jvolgeores

Mass partition during collapsing and transitional columns by using numerical simulations

Augusto Neri [a,*], Andrea Di Muro [b], Mauro Rosi [b]

[a] *Consiglio Nazionale delle Ricerche, Istituto di Geoscienze e Georisorse, Dipartimento di Scienze della Terra, Università degli Studi di Pisa, Pisa, Italy*

[b] *Dipartimento di Scienze della Terra, Università degli Studi di Pisa, Pisa, Italy*

Received 8 January 2001; received in revised form 23 August 2001; accepted 23 August 2001

Abstract

Pyroclast dispersal and mass partition between convective and collapsing transport systems represent a major issue in the understanding of the dynamics of quasi-steady explosive eruptions and the interpretation of their deposits. The spatial and temporal dispersal of pyroclasts during the initial 15 min of collapsing and transitional columns was investigated by using a transient, two-dimensional and three-phase (one gas phase and two solid phases representative of pyroclasts of varying size and density) flow model. The different behaviors of the column were simulated by using different water contents of the eruptive mixture and assuming both pressure-balanced and overpressured conditions at the vent. For each simulation results allowed the quantification of the mass of pyroclasts of different size forming the pyroclastic density current, the co-ignimbrite column and the convective plumes rising from the proximal area and above the fountain. For collapsing columns, the total mass transported in the convective system (composed of the plume above the fountain and the co-ignimbrite column) ranges from about 10 to 30 wt% of the total erupted mass according to the specific water content of the mixture at the vent. Fine particles are dominant in this convective system. With the increase of the water content the character of the column shows a collapsing/buoyant transitional behavior. Such a regime is characterized by greater collapse height, generation of more dilute density currents, shorter flow runout, less steady behavior of the column, and intermittent feeding of the flows. For these columns, the total mass forming the convective portions reaches values of up to 50 wt% of the erupted pyroclasts with a significant amount of coarse particles entrained in the convective plume above the fountain. At higher water contents the column becomes fully buoyant with the whole mass feeding the convective column. Simulations assuming overpressured conditions at the vent are characterized by more unsteady dynamics of the dispersal process with significant variations in the collapse height of the column, mass flow-rate of the flow and amount of mass elutriated in the convective system. Simulation results suggest that Plinian columns that undergo a transition from convective to collapsing regimes, as a consequence, in our case, of a water content decrease in the magma (but not necessarily limited to this case), would be characterized by a gradual decrease of the carrying capacity of the convective column above the fountain and by the emplacement of pyroclastic density currents which evolve from dilute to dense, gradually increasing their runout.

Keywords: mass partition; eruption dynamics; collapsing columns; transitional columns; multiphase flow model

* Corresponding author. Fax: +39-050-500675. *E-mail address:* neri@dst.unipi.it (A. Neri).

0377-0273/02/$ – see front matter
PII: S0377-0273(01)00304-3

1. Introduction

Pyroclastic particles erupted during magmatic explosive eruptions are dispersed into the atmosphere by very different transport systems (Fig. 1). In the convective regime, the pyroclastic mixture ejected from the crater is transported as a buoyant Plinian column up to the stratosphere until a neutral buoyancy level is reached. On the other hand, in the collapsing regime, the eruptive mixture pours in to density currents which move on the ground away from the crater for several kilometers. Large convective columns, called co-ignimbrite or phoenix columns, can rise above the flows high in the atmosphere. Both eruptive styles have been described by field studies, laboratory analogue experiments, and theoretical works (see e.g. Sparks et al. (1997) for a review). In addition to these two end-member regimes, stratigraphic studies (Walker and Croasdale, 1970; Carey and Sigurdsson, 1987; Rosi et al., 2001), physical models (Neri and Dobran, 1994; Neri et al., 1998), and laboratory experiments (Carey et al., 1988; Woods and Caulfield, 1992; Veitch and Woods, 2000) provide evidence of the existence of an intermediate regime, the transitional regime, characterized by the occurrence of simultaneous feeding of convective columns and density currents (partial collapse) and, more generally, by an unsteady behavior of the column.

Despite this large number of studies, the quantification of pyroclast dispersal and therefore of mass partitioning between the different transport systems forming the eruptive event remains difficult. The analysis of volcanic deposits alone is not actually able to provide a quantitative interpretation of the dynamic processes leading to their formation. Similarly, analogue experiments have difficulties in scaling real eruptions and mainly focus on specific aspects or processes.

The aim of this paper is to illustrate how numerical simulations using a transient, two-dimensional, three-phase fluid flow model can be employed to obtain quantitative information about the relative dispersal of pyroclasts into the different transport systems. The main advantages of this approach lie in the two-dimensional feature of the model, which allows the modeling of both the eruptive jet and the convective/collapsing portions of the dispersal process, and in the two-phase description of particles, which permits the analysis of the behavior of pyroclasts of different sizes. In addition, the transient formulation of the model allows some investigation of the unsteady behavior of the process.

As a consequence, the model is able to reproduce the various transport systems and identify the different sources of pyroclast dispersal. In particular, the partition of the erupted mass between the convecting system, formed by the plume above the fountain and the co-ignimbritic column, and the pyroclastic flow sub-domains is computed as a function of time. The method is applied here to the analysis of collapsing and transitional columns, since both are characterized by quite complex dynamics, that can be effectively described by using the fluid dynamic model adopted.

2. Overview of the physical model

The three-phase flow model of Neri and Macedonio (1996) allows the description of the dispersal of a pyroclastic mixture of two solid particulate phases, with different diameters and densities, and a hot water vapor phase in a still and dry stratified atmosphere. The governing transport equations consist of conservation equations of mass, momentum, and energy, which are solved for the gas phase and the two particulate phases on an axi-symmetric computational grid. Closure is obtained by constitutive equations, such as equations of state, viscous tensors, and semi-empirical momentum, and heat transfer coefficients between the phases. No mass transfer is allowed among the three phases. The gas is assumed to obey the ideal-gas law and solid particles are considered to be spherical and incompressible. Viscous effects in the gas phase have been accounted for by an effective eddy viscosity model able to parametrize the effects of the small-scale (subgrid-scale) turbulent motions, whereas solid phases were considered inviscid. Drag coefficients between gas and solid particles are based on well-established semi-empirical correlations. Drag due to collisions between solid phases of different sizes

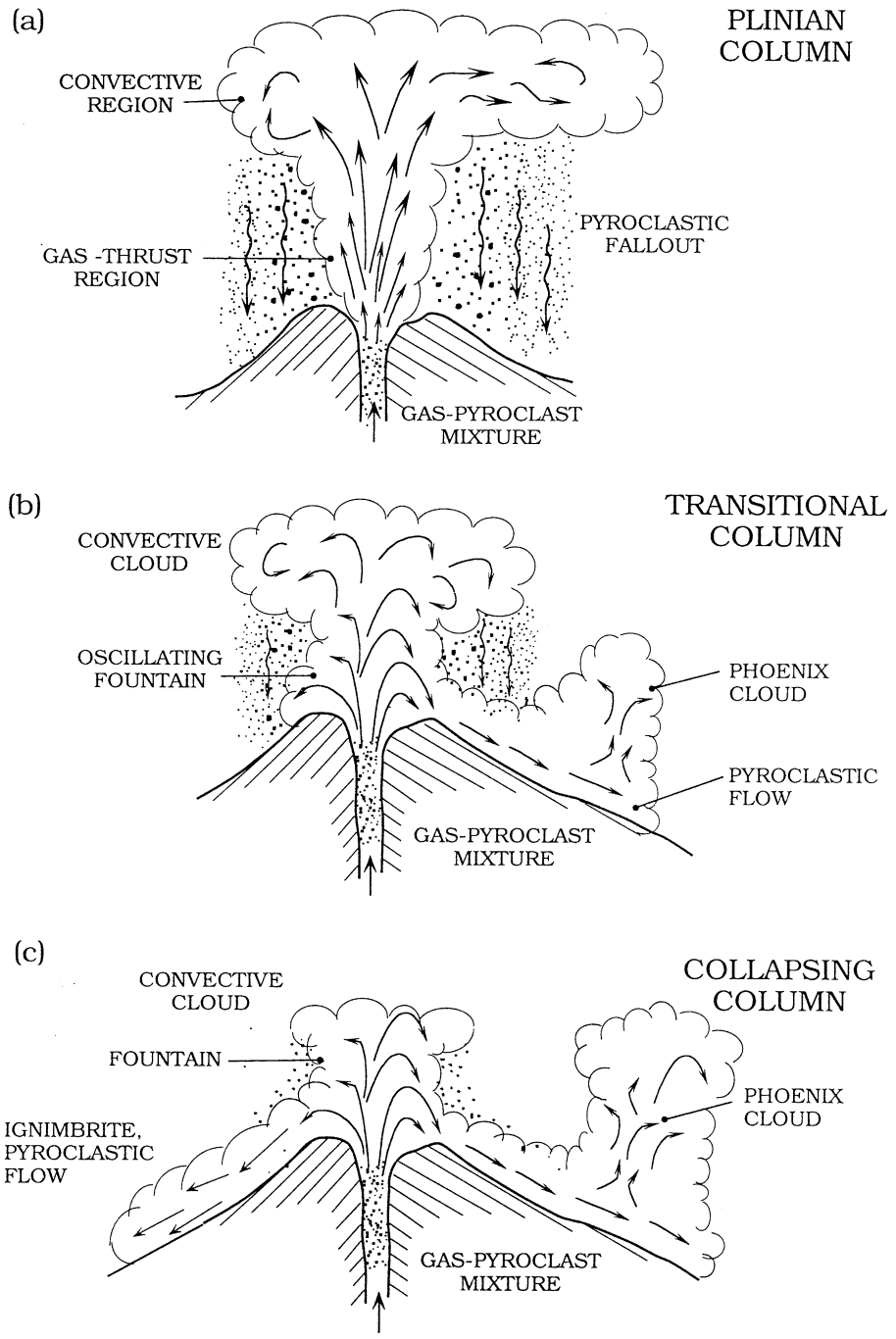

Fig. 1. Schematic illustration of three different styles of explosive eruptions: (a) a convective Plinian column, (b) a transitional column and (c) a collapsing column with formation of pyroclastic flows and co-ignimbritic clouds.

Table 1
Vent conditions of the first set of simulations

Run	Y (wt%)	T_v (K)	D_{cr} (m)	$\dot{m}$ (kg/s)	P_v bar)	v_m (m/s)	ε_g	ε_1	ε_2	ρ_m (kg/m^3)
A1	1.8	1123	600	4×10^8	1.0	133	0.9926	2.2×10^{-3}	5.2×10^{-3}	11.0
B1	2.5	1123	600	4×10^8	1.0	184	0.9947	1.6×10^{-3}	3.7×10^{-3}	7.6
C1	2.8	1123	600	4×10^8	1.0	206	0.9953	1.4×10^{-3}	3.3×10^{-3}	6.8
D1	3.0	1123	600	4×10^8	1.0	221	0.9956	1.3×10^{-3}	3.1×10^{-3}	6.0

The vertical line divides the independent (left) from the dependent (right) variables.

is also based on approximated semi-empirical correlations valid for dilute mixtures. Heat exchange between phases is allowed to occur as well. An effective thermal conductivity is assumed for the gas phase and a heat transfer coefficient is prescribed for heat exchange between solid and gas phases. Heat exchange between solid phases and viscous dissipation effects are ignored because they are insignificant in comparison to exchange due to convection, turbulent conduction, and gas–particle heat exchange (Valentine and Wohletz, 1989). Balance and constitutive equations were solved by using a semi-implicit finite difference procedure specifically designed for multiphase flows (Harlow and Amsden, 1975). The runs were performed adopting computational domains extending a few tens of kilometers in both radial and vertical directions and for about 15 min of real time. The employed computational grids were non-uniform with a minimum grid size of 5 m in the vent region and along the ground boundary. We refer to the original paper for a more detailed presentation of model equations and solution procedure (Neri and Macedonio, 1996).

3. Simulations performed

The different styles of atmospheric dispersal, from collapsing to buoyant Plinian, were investigated by prescribing different water contents to the eruptive mixture leaving the vent. Water content has been recognized as a critical magma property able to strongly affect ascent dynamics in the conduit and pyroclast dispersal into the atmosphere (Wilson et al., 1980; Woods, 1988; Papale et al., 1998; Neri et al., 1998). The influence of water vapor content on the eruptive style of the column was investigated according to two different strategies resulting in two different sets of simulations.

In both simulation sets, the pyroclastic mixture was described by means of two particulate phases with diameters of 30 and 500 μm, each accounting for 50 wt% of the whole solid mass erupted. Their densities were fixed at 2400 and 1000 kg/m^3, respectively, to take into account that the actual glass shards and crystal fragments forming the fine ash fraction have a density larger than the coarser vesiculated pyroclasts. Despite this simple representation of the eruptive mixture, the two particle phases chosen can give useful indications about the dispersal process of the coarser and finer portions of the real eruptive mixture, as shown by simulations adopting a multiparticle formulation of the solid phase (Neri et al., 2001). Mechanical and thermal equilibrium was assumed at the vent between the two solid phases and the water vapor phase in all runs.

In the first set (see Table 1), atmospheric pressure-balanced conditions were assumed as inlet boundary conditions of the column. Specifically, we considered the injection of a supersonic pressure-balanced jet, with a diameter of 600 m and no elevation above the ground, into the atmosphere. In this case, the assumed boundary conditions are representative of the jet conditions after its decompression in the volcanic crater. The reasonableness of this assumption comes from previous studies on the dynamics of overpressured jet (Woods and Bower, 1995; Neri et al., 1998) indicating the production of a supersonic flow at about atmospheric pressure just a few hundred meters above the conduit vent. Four runs were carried out with a constant mass flux of 4×10^8 kg/s, temperature of 1123 K, and water

Table 2
Vent conditions of the second set of simulations

Run	Y (wt%)	T_v (K)	D_{cr} (m)	$\dot{m}$ (kg/s)	P_v (bar)	v_m (m/s)	ε_g	ε_1	ε_2	ρ_m (kg/m^3)
A2	2.2	1150	527	3.8×10^8	28	148	0.8593	4.14×10^{-2}	9.93×10^{-2}	203
B2	2.6	1150	527	4.9×10^8	49	159	0.8321	4.94×10^{-2}	11.85×10^{-2}	243
C2	3.3	1150	527	6.3×10^8	60	181	0.8127	5.51×10^{-2}	13.22×10^{-2}	273
D2	4.0	1150	527	7.2×10^8	76	198	0.8033	5.79×10^{-2}	13.88×10^{-2}	289

The vertical line divides the independent (left) from the dependent (right) variables.

content ranging from 1.8 to 3.0 wt%. In this case, the volume fractions of the three phases at the vent and the mixture velocity were calculated simply through the mass conservation equation alone as a function of the given mass flux, pressure, temperature and water content assumed. In this way, despite neglecting the true decompression dynamics of the jet, it is possible to produce the convective/collapsing transition of the column at constant mass flow-rate and therefore to highlight the net effect of water content on column dynamics.

In the second set (see Table 2), the decompression of the pyroclastic mixture erupted from a vent 127 m wide was simulated in a crater 200 m high and with an inner slope of 45° (thus resulting in a crater diameter of 527 m). In this case, the dependence of the vent parameters on the water content was taken into account by using the output data of the simulations of the ascent of an aphiric dacite magma by Papale et al. (1998) as vent conditions (runs calc14, 15, 16, and 17). As a result, mass flow-rate and exit pressure are no longer independent variables, but vary as a function of water content. Four simulations were carried out with a constant temperature of 1150 K and a water content that ranges from 2.2 to 4.0 wt% producing a range of mass flow-rate from 3.8 to 7.2×10^8 kg/s and of exit pressure from 2.8 to 7.6 MPa. Since only one class of solid particles with constant diameter and density was considered in the study of Papale et al. (1998), those vent conditions were slightly modified to accommodate the presence of two solid phases with different densities. This was achieved by assuming that the exit pressure remains constant and recomputing the volume fractions of the three phases according to the mass conservation equation.

4. Pyroclastic dispersal results

Before presenting the mass partition analysis, a general description of the large-scale dispersal will be given for selected runs pertaining to both eruption sets described above.

4.1. Pressure-balanced jets

Fig. 2 shows the evolution of the 30-μm (left) and 500-μm (right) particle volumetric fractions of Simulation A1 characterized by the lowest water content considered. Fig. 3 (left) reports the corresponding evolution of the total particle volumetric fraction of the same simulation. As we will see, this eruption is representative of the collapsing regime and clearly identifies the different transport systems governing the dispersal process, such as the pyroclastic flow and the convective plumes above the flow and the fountain.

The vertical injection of the jet into the atmosphere is characterized by a decrease in its density due to entrainment of atmospheric air and expansion in the pressure-stratified atmosphere. Once the mixture height has reached about 1 km, part of the mixture retains a density higher than the surrounding air and moves towards the ground, whereas the lighter portion ascends buoyantly into the atmosphere (see 100 s). The collapsed stream splits into two portions: the first feeds an outward moving density current and the second merges back into the recycling fountain. The buoyant plume above the fountain is fed unstead-

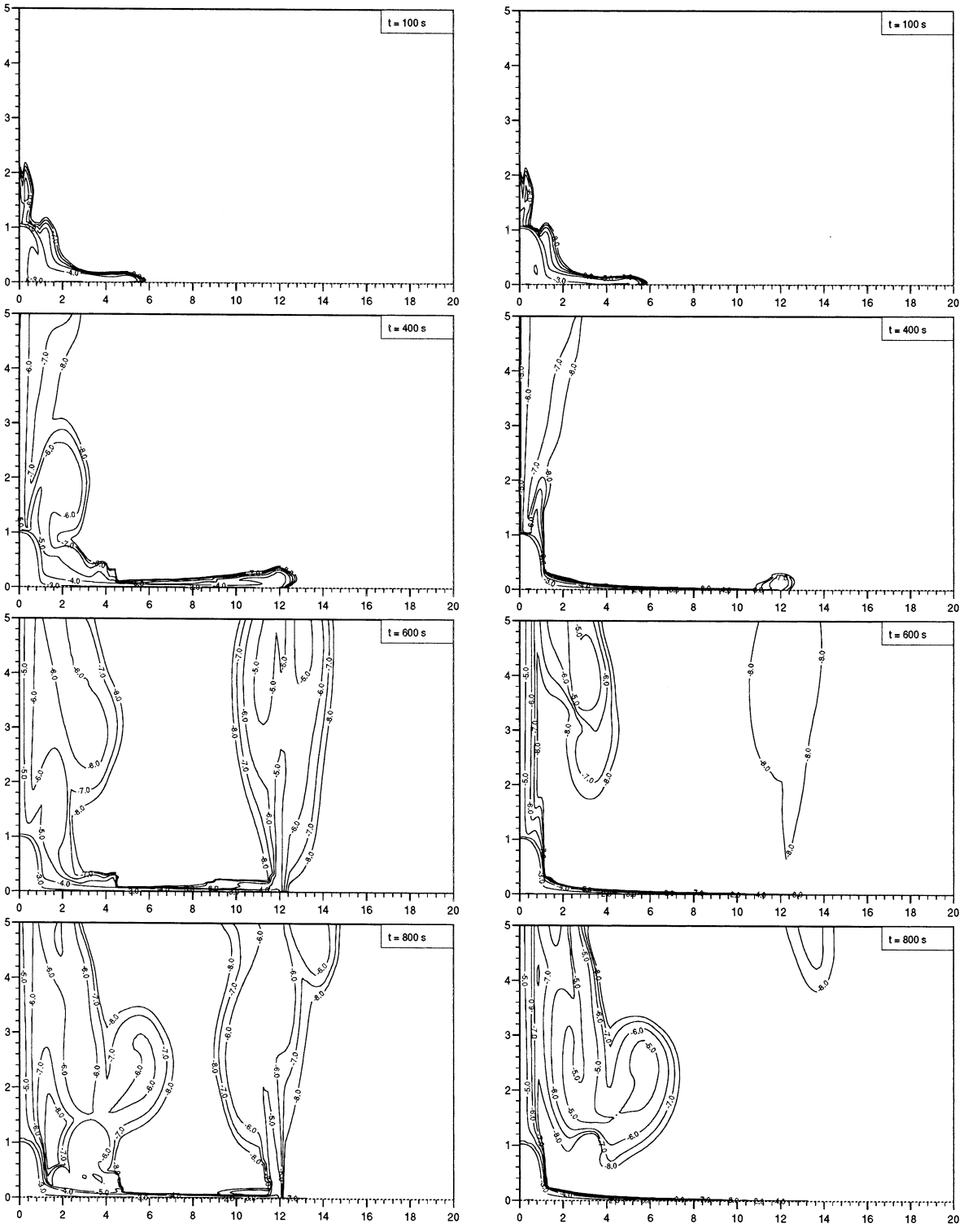
t = 100 s
t = 400 s
t = 600 s
t = 800 s
t = 100 s
t = 400 s
t = 600 s
t = 800 s

ily by diluted vorticose mass pulses which rise from the edge of the fountain, where the mixing with the atmosphere is more effective, and merge towards the column axis. Later on (400 s), discrete dilute plumes, here called thermals, rise convectively from the pyroclastic current near the area of impact of the fountain with the ground (deflation zone) and merge into the convective plume above the fountain. Both 30- and 500-μm particles are transported in similar proportions in the plume above the fountain, whereas almost only 30-μm particles are carried upward by the convective thermals.

At the same point in time, the outward moving pyroclastic density current has reached a distance of 12 km from the vent. During propagation the current body is about 200–300 m thick. The two solid phases are concentrated mostly in the lower portion of the flow, producing a strong gradient of mixture density and particle concentration. The upper diluted portion of the flow has a density lower than the surrounding atmosphere and it does not rise buoyantly until the current travels at high speed. The 500-μm particles are almost totally concentrated in the basal, about 15-m-thick, dense layer, where they account for up to 80 wt% of the total solid load, whereas the 30-μm particles account for up to 95 wt% in the upper and more diluted portion of the pyroclastic density current.

At about 450 s (not shown), a convective co-ignimbritic column starts to rise above the head of the pyroclastic flow and during the ascent it progressively expands upwards until it joins with the convective central plume above the fountain at 850 s (see distributions at 600 and 800 s). In the co-ignimbrite column, the 30-μm particles account for almost the whole solid load. After the development of the co-ignimbrite column, the density current does not propagate further, attaining a maximum runout of about 12 km from the vent, probably due to the strong winds induced by the rising plumes above the fountain and the pyroclastic flow.

The increase in water vapor content of the erupted mixture produces marked changes in the dispersal dynamics. As in Simulation A1, both a convective column ascending above the fountain and a pyroclastic density current continuously fed by the fountain are simultaneously produced during Simulations B1 and C1, carried out with water contents of 2.5 and 2.8 wt%, respectively. On the other hand, a small density current is generated only during the early phase of Simulation D1 (with 3.0 wt% of water vapor) that later on produces a fully convective column.

Fig. 3 (right) illustrates the evolution of the total volumetric particle fraction of Simulation C1 in order to show the main changes to the large-scale dynamics. As discussed later on, this simulation can be considered representative of the transitional regime. The first significant change regards the collapse height of the column, which increases with the water vapor content reaching a value of 3 km for Simulation C1 (see 100 s). The collapse height also begins to oscillate slightly in time producing more unsteady behavior of the fountain. In addition, the collapsing stream feeds a more dilute and expanded pyroclastic current with respect to Simulation A1. The thickness of the body of the flow increases up to about 400–500 m in Simulation C1, and is about twice the value produced by Simulation A1 (400 s). Marked gradients of particle concentration, mixture density and temperature of the phases develop similarly as in the A1 run. The volumes of the buoyant plume that ascends above the fountain, of the thermals that rise above the flow, and of the phoenix columns forming at the flow head also increase as a function of the water content (600 s). The co-ignimbrite column formed at the flow front is more diluted and cooler than the convective column that develops above the fountain and transports a solid load constituted for about 95 wt% of 30-μm particles. Finally, at 800 s, a voluminous convective system is generated by the merging of all buoyant plumes that rise above the density current and the fountain.

Fig. 2. Distribution of (left) the 30-μm and (right) the 500-μm volumetric fraction at 100, 400, 600, and 800 s of Simulation A1. The contour levels shown are the exponents to the base 10 and correspond to −8, −7, −6, −5, −4, −3, −2, and −1.

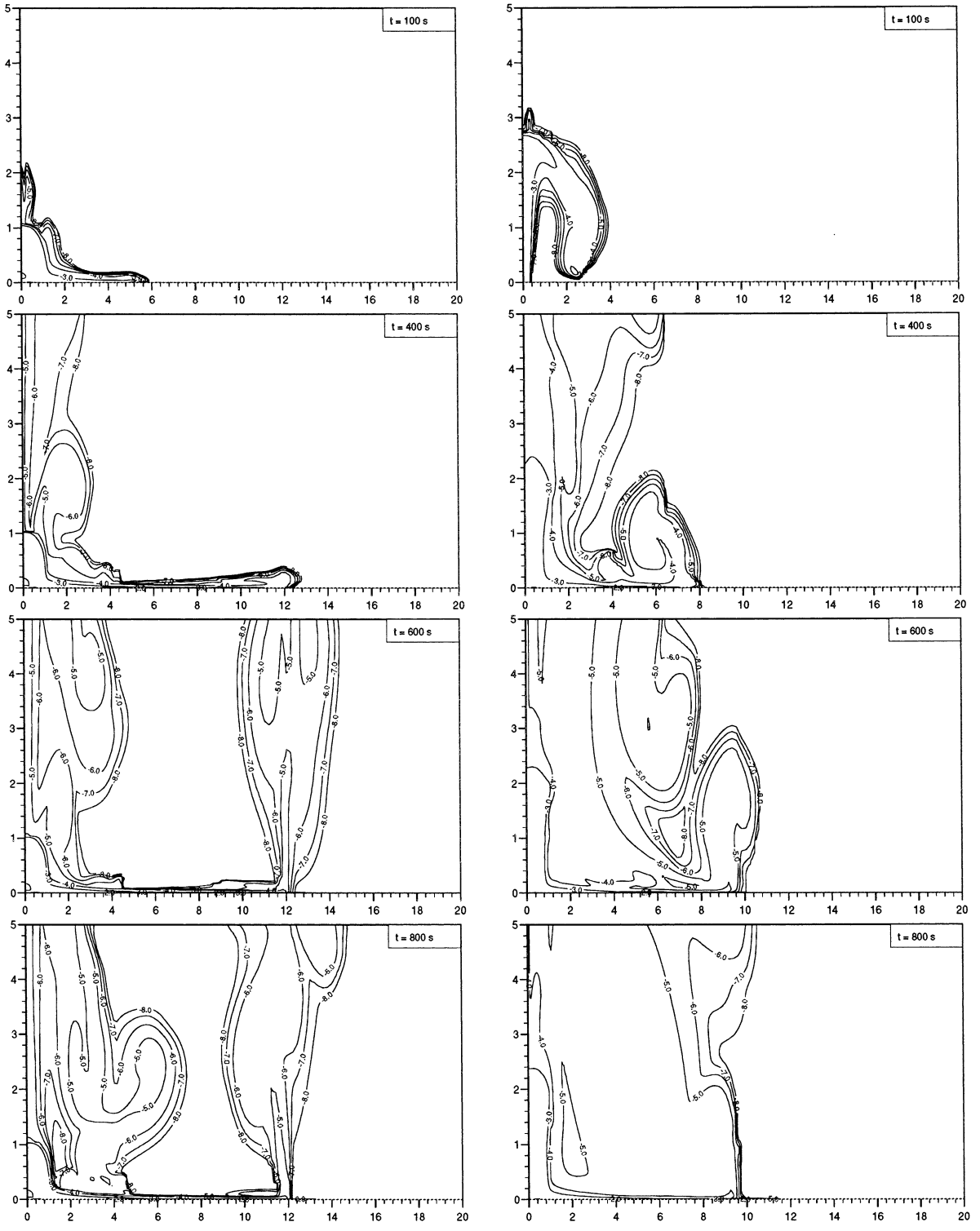
t = 100 s
t = 100 s
t = 400 s
t = 400 s
t = 600 s
t = 600 s
t = 800 s
t = 800 s

The final runout of the flow is about 2 km shorter than that of Simulation A1.

4.2. Overpressured jets

Similarly to Fig. 3 discussed above, Fig. 4 illustrates the temporal distribution of the total volumetric particle fraction of Simulations A2 and C2, performed by using results of magma ascent models. In this case the pyroclastic mixture is erupted from a conduit vent and decompresses and expands radially in a crater. Decompression waves propagate from the conduit vent edge, reflect as oblique waves on the external surface of the jet and generate a shock normal to the symmetry axis (Mach disk) in all simulations. The excess pressure of the mixture at the vent strongly affects the dynamics of the jet, fountain, and convecting/collapsing streams producing considerable unsteadiness in the dispersal process much greater than that observed in the first set of pressure-balanced simulations.

Fig. 4 (left) illustrates the behavior of Simulation A2 carried out with the lowest water content. Again, at the top of the jet, the portion of the mixture that is lighter than the surrounding air rises buoyantly into the atmosphere, while the denser portion moves towards the ground (100 s). Both fountain height and width strongly oscillate in time. As in the pressure-balanced runs, the convective system above the fountain is fed by large vorticose pulses that rise mostly from the edge of the fountain and merge towards the plume axis with a characteristic period of about 100 s, shorter than in the first set of simulations. Similar amounts of fine and coarse particles are transported in this system.

A significant difference of set 2 from set 1 is the almost continuous buoyant clouds rising above the pyroclastic density current fed from the collapsing fountain (400 s). As a consequence, the pyroclastic flow, during its propagation, is wedge-shaped and characterized by the development of many discrete thermals, with a period ranging from 25 to 100 s, above its proximal and medial portion. Eventually, these plumes merge into the main plume ascending above the fountain. The physical properties of these thermals change as a function of the distance from the crater. Proximal thermals are hotter and richer in water vapor and 500 μm particles than the distal ones.

At 600 s, a lobate and not clearly defined coignimbrite column begins to be fed from the upper layers of the density current between 5 and 9 km from the crater, about 5 km behind the flow head. At 950 s, the phoenix column merges with the large column above the fountain. At that point in time, the flattened shape of the more distal part of the flow is due to the strong winds blowing in the direction of the crater, caused by the ascent of the buoyant plumes. The final flow runout is greater than 21 km. The pyroclastic flows fed by the collapsing overpressured jets are also more unsteady than those produced in the first set of pressure-balanced simulations, however, they show similar vertical and lateral gradients of particle concentration, mixture density and temperature.

A progressive transition towards more buoyant columns, i.e. the ability to carry larger quantities of solid pyroclasts and hot water vapor, is again obtained by increasing the magma water content. This transition is associated with an even stronger unsteadiness of the fountain and of the density current as compared to the first set of simulations. As an example, Fig. 4 (right) illustrates the behavior of Simulation C2 at the same four times as Simulation A2. The height of the collapse and the initial distance of impact with the ground increase in the more buoyant eruptions and they also become more oscillating in time. As a consequence, the pyroclastic flow is no longer fed continuously by the fountain, but by several discrete pulses with a period ranging between 50 and 300 s. The flow runout is also reduced with respect to

Fig. 3. Distribution of the total particulate volumetric fraction at 100, 400, 600, and 800 s of (left) Simulation A1 and (right) Simulation C1. The contour levels shown are the exponents to the base 10 and correspond to −8, −7, −6, −5, −4, −3, −2, and −1.

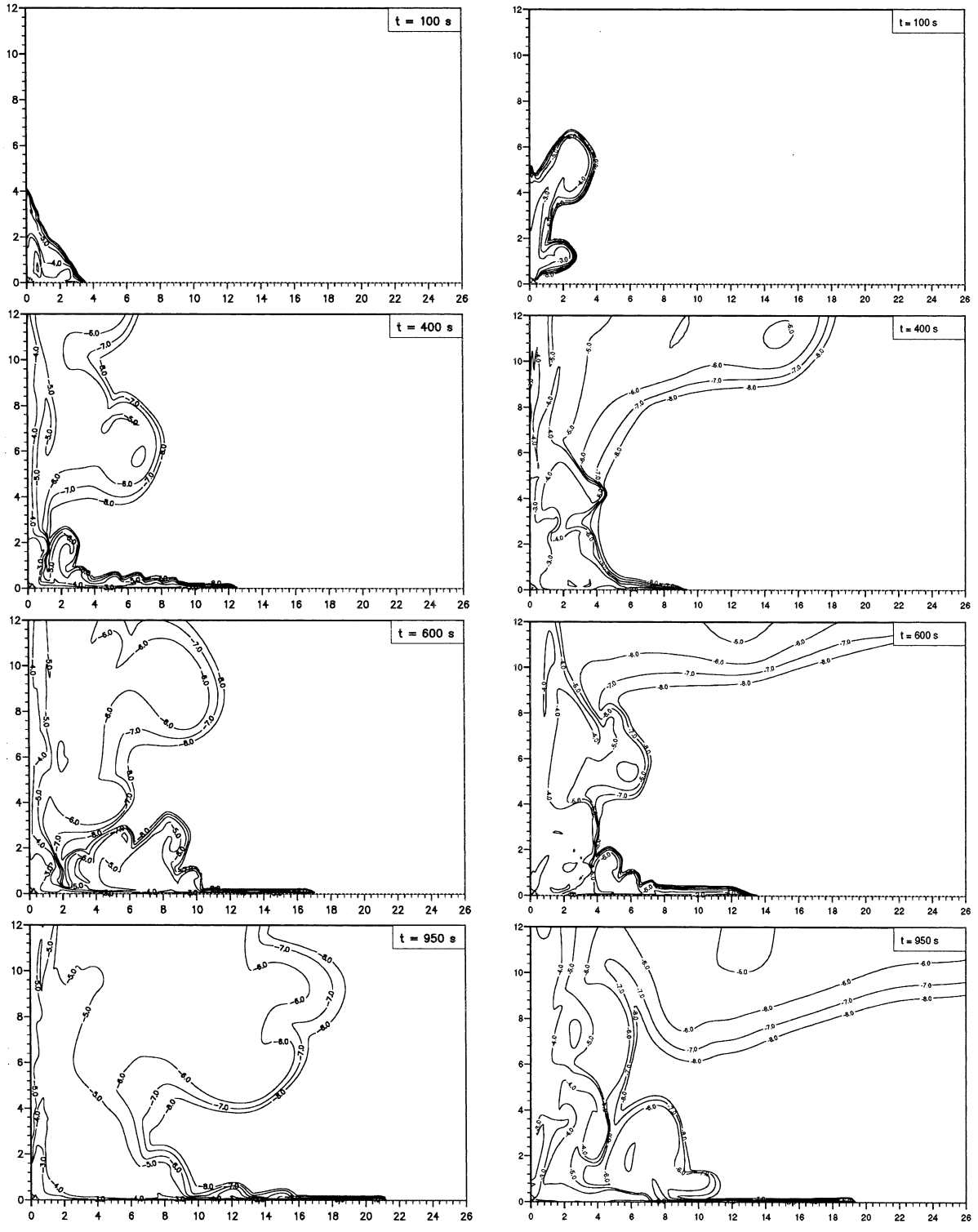
t = 100 s
t = 100 s
t = 400 s
t = 400 s
t = 600 s
t = 600 s
t = 950 s
t = 950 s

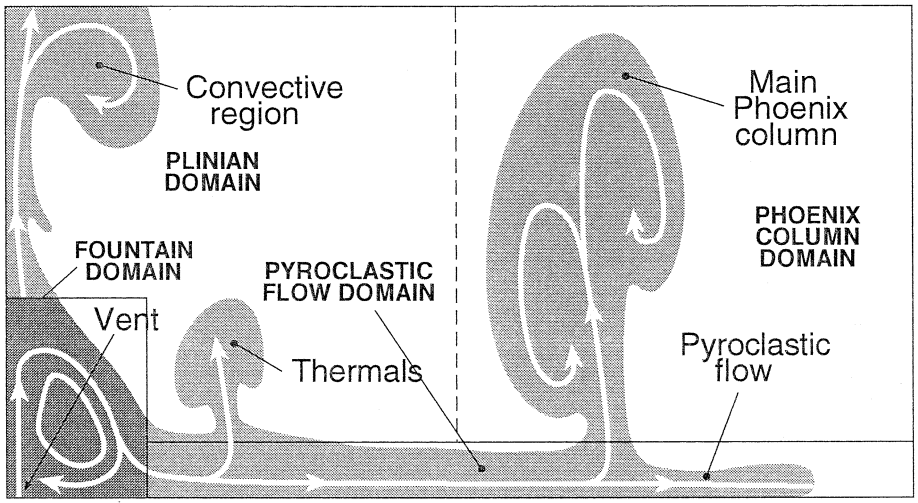

Fig. 5. Sketch of pyroclastic dispersal systems and computational sub-domains defined to estimate the pyroclast mass partition (modified from Neri and Dobran, 1994).

Simulation A2. No major co-ignimbrite column is fed, in this simulation, by the density current, but only short-lived thermals form. The more proximal thermals are clearly correlated to the extremely unsteady behavior of the collapsing stream. All this produces a more effective transport of both fine and coarse particles into the convective plume above the fountain. Finally, Simulation D2, carried out with the highest water content, produces a short-lived collapse (about 40 s) feeding a small and dilute density current.

5. Mass partition

Simulation results will now be analyzed in order to quantify the relative amount of pyroclasts in the different transport systems. To do this, the physical domain simulated has been subdivided into four sub-domains, i.e. (1) the fountain domain; (2) the pyroclastic flow domain; (3) the buoyant Plinian domain; and (4) the phoenix column domain (see Fig. 5). Boxes with constant height and width were defined for both simulation sets to calculate, as a function of time, the fractions of the two particulate phases which are present in the defined regions of space with respect to the total amount erupted from the vent. In particular, a box 4 km high and 1.5 km wide was selected to quantify the mass present in the fountain and a box 0.5 km high and extended from 1.5 km from the vent to the end of the domain was utilized for the pyroclastic density currents. The solid mass transported into the whole convective system, i.e. the Plinian plus phoenix column domains, was calculated as a difference between the total erupted mass and the mass located in the fountain plus pyroclastic flow domains. Only in a few cases, i.e. when the phoenix column was clearly distinguishable, Plinian and phoenix fractions were quantified separately.

Fig. 6 shows the fraction of erupted pyroclasts present in (a) the fountain domain and (b) the pyroclastic flow domain as a function of time, for the first set of simulations. Solid and dashed lines refer to 30 and 500 μm, respectively. During the initial 30 s, the whole erupted solid mass is

Fig. 4. Distribution of the total particulate volumetric fraction at 100, 400, 600, and 800 s of (left) Simulation A2 and (right) Simulation C2. The contour levels shown are the exponents to the base 10 and correspond to −8, −7, −6, −5, −4, −3, −2, and −1.

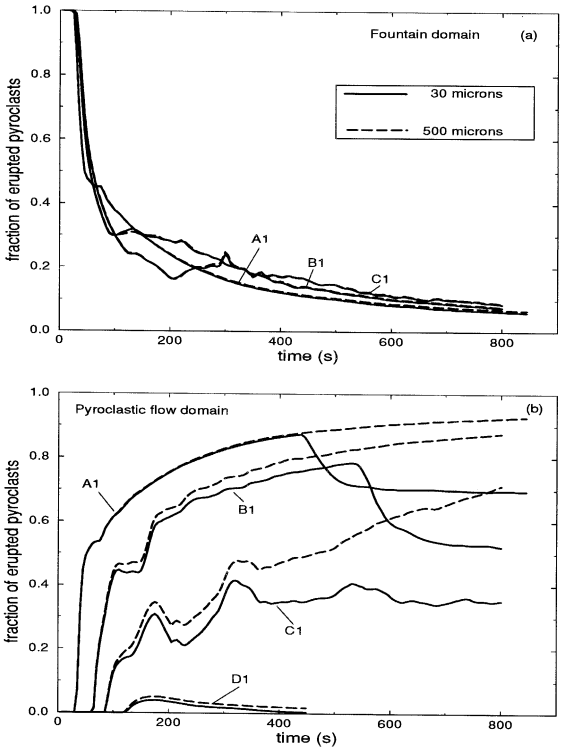

Fig. 6. Timewise distribution of the (a) fountain and (b) pyroclastic flow mass fractions of the 30-μm (solid lines) and 500-μm (dashed lines) particles as computed for the first set of simulations.

contained inside the box of the fountain, as shown in Fig. 6a. Subsequently, the mass fraction of both particles located in the fountain domain rapidly decreases as an increasing fraction of particles feeds the propagation of the pyroclastic flows and the ascent of the convective plume above the fountain. No appreciable difference between fine and coarse particles is observed in the four runs, indicating that the fountain is a well-mixed system unable to actually separate the two particle types. At 400 s the fraction of mass contained in the fountain box is lower than 0.2, whereas at 800 s it is lower than 0.1. Clearly, further along in the eruptions, when a large amount of mass has been erupted, such a contribution is destined to become negligible. As a consequence, fractions computed at later times, i.e. about 800 s in our simulations, are the ones more representative of the long-term behavior of the system.

Fig. 6b shows the fraction of erupted pyroclasts partitioned in the pyroclastic flow domain. As previously discussed, the A1, B1 and C1 pyroclastic flows are fed continuously by the fountain, while the D1 current is produced by an initial brief collapse of the column, which later on evolves into fully convective Plinian behavior. In the continuously fed currents, the fraction of both the erupted particles that pours into the current increases until the co-ignimbrite column develops, that is, at about 450 s in the A1 and about 550 s in the B1 and C1 runs. Larger fractions clearly correspond to lower water contents of the mixture. Before the generation of the phoenix, the difference in content between the two particle phases is a function of the development of buoyant thermals which mainly elutriate the-30 μm particles from the density current. As a consequence of the formation of the phoenix column, a large amount of 30-μm pyroclasts is subtracted from the flow, while the content of the 500-μm particles continues to increase. At about 800 s, an almost constant fraction of both erupted solid particles is reached for Simulations A1 and B1, whereas Simulation C1 still shows an increasing trend for the coarse pyroclasts. Specifically, about 95, 90, and 70% of 500-μm particles and 70, 50, and 35% of 30-μm particles are present in the flow in Simulations A1, B1, and C1, respectively. The trend of variation of the solid mass content is quite smooth in the A1 current, which feeds only small and diluted thermals, and it becomes progressively more unsteady in the B1 and C1 simulations, performed with a higher water content. The final percentage of the total erupted solid mass that has been poured into the pyroclastic flow decreases from about 80 wt% in the A1 run performed with the lowest water content, to 70 wt% in the B1 run and to 50 wt% in the C1 run.

The fraction of particles elutriated into the convective system defined above is shown in Fig. 7a. The increase in the water content in the erupted pyroclastic mixture produces a progressive transition from a collapsing column (Simulation A1) to a convective regime (Simulation D1). The final fraction of the total erupted solid phase poured

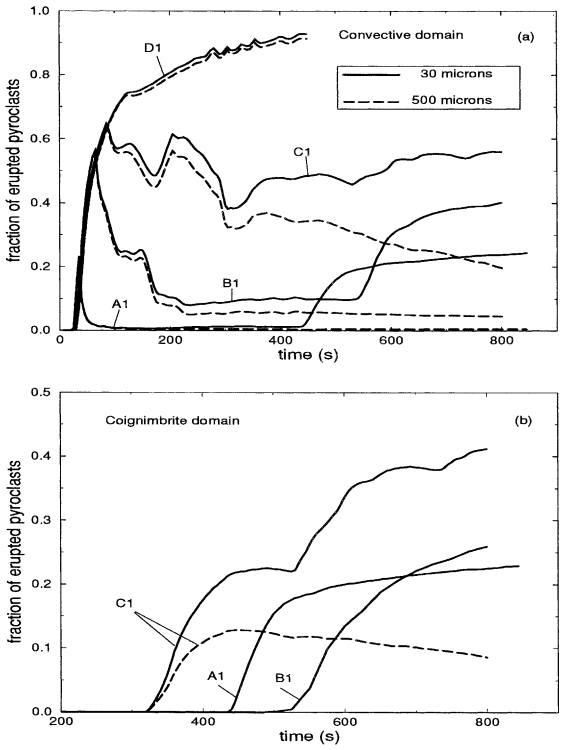

Fig. 7. Timewise distribution of the (a) total convective and (b) phoenix mass fractions of the 30-μm (solid lines) and 500-μm (dashed lines) particles as computed for the first set of simulations. The phoenix fraction is shown only for Simulations A1, B1, and C1 since the column was not formed in Simulation D1.

in the whole convective system increases from about 10 wt% (A1), to 20 wt% (B1), to 40 wt% (C1) to 90 wt% (D1). From the figure it is again possible to observe the elutriation of particles from the plume above the fountain and the thermals ascending above the current (before the development of the co-ignimbrite column), the rapid increase in the content of the 30-μm particles due to the ascent of the phoenix column, and the increase in the fraction of fine and coarse particles transported by the convective system in the simulations carried out with the higher water content. Fig. 7b illustrates the temporal behavior of the particle fraction elutriated into the phoenix column for Simulations A1, B1, and C1. It should be noted that, whereas it is possible to clearly distinguish the specific mass contribution of the co-ignimbritic column of Simulations A1 and B1, the quantification of this fraction is more difficult for Simulation C1 due to the early merging of the phoenix column with the proximal thermals and the plume above the fountain. However, it is evident from the figure that the amount of mass elutriated into the phoenix column increases with the increase of water and that a significant amount of coarse particles can be transported by the rising plume.

Fig. 8 shows the fraction of erupted pyroclasts present in (a) the pyroclastic flow domain and (b) the whole convective domain, for the second set of simulations. The behavior of the fountain fraction is analogous to the one shown in Fig. 6a and is not reported here. As shown, the decompression of an overpressured jet produces more unsteady dynamics of both the plume above the fountain and the pyroclastic density current than that observed in the first set of pressure-balanced simulations. The effect of the greater unsteadiness

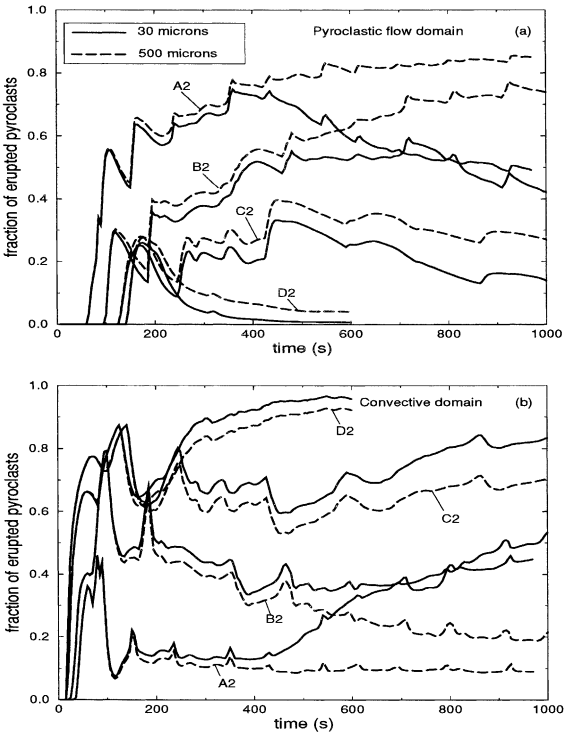

Fig. 8. Timewise distribution of the (a) pyroclastic flow and (b) convective mass fractions of the 30-μm (solid lines) and 500-μm (dashed lines) particles as computed for the second set of simulations.

can clearly be recognized in the temporal trends of the mass partition between the density current and the convective system.

As in the first set of runs, the density current is continuously fed during the more collapsing Simulations A2 and B2, whereas intermediate behavior is observed in Simulation C2 in which the flow is fed by short-living pulses, with a duration decreasing in time (see Fig. 8a). Simulation D2 performed with the highest water content again feeds a small and diluted density current only during the early phase of the eruption and is therefore representative of a buoyant Plinian column. In the continuously fed A2 and B2 density currents, the fraction of both erupted solid particles poured in the flow increases until the time of ascent of the phoenix. Before this time (400 s in the A2 run, 600 s in the B2 run), the moderate difference in content between the 30- and 500-μm pyroclasts is due to the elutriation from the flow by the buoyant thermals that mainly carry on the small particles and it increases in the runs performed with the higher water content. When the transitional regime is approached, the feeding of the flow becomes increasingly pulsatory. At the end of the simulations, almost constant values of 85, 75, and 30% of 500-μm particles and 50, 40, and 15% of 30-μm particles are predicted in the flow of Simulations A2, B2, and C2, respectively. The percentage of the whole solid load poured in the pyroclastic flow decreases from about 70 wt% (A2), to 60 wt% (B2), to 25 wt% (C2).

Fig. 8b illustrates the same trend from collapsing, to transitional, to convective regime by computing the fraction of erupted mass that is transported in the whole convective system. As discussed above, these fractions are almost the complement to one of the pyroclastic flow fractions. The fraction of the total erupted solid phase poured in the whole convective system is now estimated to increase from 25 wt% (A2), to 35 wt% (B2), to 70 wt% (C2) to about 95 wt% (D2). A notable difference with respect to the first set of simulations (see Fig. 7a) is the prediction, for simulations with lower water content, of higher fraction of particles transported in the convective system due to the more effective production of thermals from the pulsatory spreading flow.

6. Discussion

In the following two sub-sections we will discuss separately the results pertaining to the dynamics of collapsing and transitional columns, even though the present study suggests a gradual transition from one style to the other. Results appear to be significantly independent of assumptions regarding the vent conditions (set 1 vs. set 2), which appear to influence the degree of unsteadiness of the dynamics, but not the large-scale behavior of the system. For each sub-section, the modeling results will be first summarized and then interpreted in the light of present understanding coming from field studies.

6.1. Collapsing columns

In the collapsing regime most erupted mass pours into the radially spreading density currents producing the highest values of density in the lower layer of the flow. However, a complex convective system is formed by the merging of plumes with different properties, coming from different locations of the fountain and density current. For the columns with lower water content, numerical simulations made it possible to distinguish between a convective plume centered on the symmetry axis of the computational domain (located in the Plinian domain of Fig. 5), and a long-lasting co-ignimbrite column (located in the phoenix column domain). The former plume is produced by the merging of a buoyant plume rising just above the fountain top and discrete, short-living thermals rising from the density current in the proximal area. Unfortunately, it was not possible to quantify the relative amount of particles transported into the two systems due to their close locations and rapid merging into a single plume.

However, the convective plume above the fountain and the co-ignimbrite column can be clearly recognized due to their markedly different locations and properties. The plume above the fountain is able to transport both coarse and fine particles and significant amounts of hot water vapor in all runs. Typically, for the range investigated, up to 10 wt% of both particles are transported in this plume (see Figs. 7a and 8b). The mass of

these particles increases when moving towards a higher water content. Simulation results indicate that part of this mass is related to the development of thermals from the proximal region of the flow, especially in the case of overpressure jets, because of the larger buoyancy and unsteadiness of the fountain and density currents. As shown by the overpressured set of runs, the formation of these plumes is strongly related to the presence of velocity and density fluctuations of the flow. The properties of the thermals change with the distance from the crater. The thermals ascending near the area of impact of the collapsing stream with the ground are fed by an expanded, diluted and hot portion of the current where the coarse particles are still largely in suspension. The distal thermals are fed by the upper and cooler layers of the flow, rich in fine particles, because the coarse ones are already concentrated near the ground. As an example, observations confirming this tendency were made at Redoubt Volcano (Woods and Kienle, 1994).

The mixture forming the distal co-ignimbrite column is richer in air, cooler and the fine particles account for about 100 wt% of the solid load. A maximum amount of about 40 wt% of the 30-μm particles erupted from the vent is elutriated in this way. Basically no coarse particles are elutriated into the phoenix (Neri et al., 2001). These predictions are fully consistent with field data which show that the co-ignimbrite deposit is mainly made up of small glass shards and can have a mass comparable to that of the related pyroclastic flow deposit (Sparks and Walker, 1977; Sigurdsson and Carey, 1989; Woods and Wohletz, 1991). The simulations also show that the mass transported in the co-ignimbrite cloud is larger in runs with higher water content.

Regarding the density currents, simulations indicate they are continuously fed by the fountain with a higher degree of unsteadiness of the flow in the case of overpressured jets. The runout of these currents is the greatest observed in the simulations performed as well as the density values predicted in the lower part of the flow. Density currents seem to be unable to effectively separate fine and coarse particles. All these features suggest that these flows result in the emplacement of pyroclastic flow-like deposits (sensu stricto), consistent with many stratigraphic observations.

6.2. Transitional columns

Previous physical models (Wilson et al., 1980; Wilson and Walker, 1987; Woods, 1988; Valentine and Wohletz, 1989) described a sharp transition from the convective to the collapsing regime as a function of vent parameters. As a consequence, the emplacement of the intraplinian density currents has commonly been related to partial collapses of the erupted mixture, synchronous with a buoyant column and produced by factors external to the dispersal dynamics. Some of these are: temporary changes in conduit or crater geometry by collapse or erosion (Walker, 1981), congestion of the vent located within a basin (Wilson and Walker, 1985), sharp and temporary changes of magma properties (Carey et al., 1990), coexistence of magmatic and hydrovolcanic fragmentation in the conduit (Valentine and Giannetti, 1995), non-homogeneity of the pyroclastic mixture produced by the explosive fragmentation process (Anilkumar et al., 1993), collapse of high concentration regions of the eruptive plume (Bacon, 1983), and particle recycling from the fall-out activity into the convective column (Veitch and Woods, 2000).

The present modeling work suggests a progressive transition from convective (Simulations D) to collapsing (Simulations A) columns. Between these two end-member regimes a transitional regime can be identified (Simulations C). This transitional region appears to be wider in the case of vent conditions based on the magma ascent modeling (second set) than in the case of constant mass flow-rate (first set). Transitional columns are characterized by the splitting of the erupted mass between a collapsing portion, producing a pyroclastic current fed by a high collapsing fountain (up to about 4 km in our runs), and a convective portion producing a buoyant plume. In particular, the buoyant plumes rising above the fountain and the proximal region of the flow (thermals and phoenix columns) are able to elutriate a considerable amount of coarse particles. The significant mass of coarse particles pouring

into the buoyant column can therefore be segregated in a fall-out activity synchronous with the emplacement of density currents.

It is important to note that the coexistence of a buoyant column and density currents has been reproduced, with steady and homogeneous conditions of the mixture at the vent, as a result of the complex and transient flow pattern characterizing the coupled fountain and atmospheric dispersal dynamics for columns close to the transition between the buoyant Plinian and collapsing regimes without any involvement of the above described external factors.

The numerical simulations also show that density currents produced by transitional columns are characterized by strong variation of mass flow-rate, velocity, and density and by a shorter runout as compared to collapsing columns. In particular, the pulses of mass pouring into the current have an increasing frequency as the simulation moves from the fully buoyant to the collapsing regime. In addition, the amplitude of the oscillations of both collapse height and radial distance of impact with the ground is significantly greater in the transitional regime as compared to the collapsing columns.

Field studies show significant consistencies with modeling results. In many explosive eruptions, covering a wide range of intensity (Bacon, 1983; Sparks et al., 1985; Wilson and Walker, 1985; Carey et al., 1990; Hildreth and Drake, 1992) and magmatic composition (Walker and Croasdale, 1970; Carey and Sigurdsson, 1987; Valentine and Giannetti, 1995; Bourdier et al., 1997; Bertagnini et al., 1998), density current deposits are found interstratified with the fall-out bed. In some other cases, the fall-out activity and the emplacement of the density currents have been interpreted as synchronous during the whole eruption (Fierstein and Hildreth, 1992; Wilson and Hildreth, 1997). In addition, the large unsteadiness observed in our numerical simulations as well as the low density of the predicted density currents are consistent with the emplacement of intraplinian surge-like deposits (Wilson and Walker, 1985; Wilson and Hildreth, 1997). The increase in frequency of the collapse episodes moving from the fully buoyant towards the collapsing regime is also consistent with an increase in the number of intraplinian deposits observed before the full collapse of the erupted mixture (Walker, 1981; Rosi et al., 2001).

Finally, these results appear to be consistent with laboratory experiments performed using particle-laden plumes of fresh water in a tank of salt water (Carey et al., 1988) and mixtures of methanol and ethylene glycol (Woods and Caulfield, 1992). These experiments, with appropriate conditions at the vent, reproduce the coexistence of a buoyant plume with the emplacement of density currents and the unsteady feeding of a convective transport system. The existence of a range of possible collapse behavior with increasing unsteadiness in the transitional regime has been also reproduced by those experiments.

7. Summary and conclusions

The numerical simulations of pyroclastic dispersal carried out with the adopted transient, two-dimensional and three-phase flow model enabled us to investigate the dynamics of collapsing and transitional columns and, in particular, the mass partition among different transport systems. Different eruptive styles were reproduced by varying the water content of the mixture at the vent, keeping constant the mass flow-rate or adopting vent conditions derived from modeling magma ascent.

Regarding collapsing columns, our simulations make it possible to distinguish clearly between collapsing and convective systems. For these columns about 70–80 wt% of the erupted mass forms the radially spreading density current, whereas the remaining 20–30 wt% is elutriated mainly from the phoenix column which is able to elutriate about 40% of 30-μm particles. The formation of a plume above the fountain and thermals from the more proximal region of the flow were also recognized as secondary elutriation systems for collapsing columns and were not able to drag a significant amount of coarse particles.

At higher water contents the column behavior is transitional and characterized by more complex dynamics. These columns can feed both convec-

tive rising plumes and pyroclastic density currents, thus splitting the erupted mass into comparable amounts between the collapsing and convective regions. For these columns the segregation between coarse and fine particles appears to occur during the collapse phase itself, as well as during the proximal propagation of the flow. However, these columns are characterized by the presence of a considerable amount of coarse particles in the convective plumes rising from the fountain and the proximal region of the flow. With respect to collapsing columns, transitional columns are characterized by more unsteady dynamics including the possibility of alternating/coexisting feeding of collapsing and convective streams. The transition between full collapsing and convective regimes appears to occur through a water content change of about 0.5/1.5 wt% with the larger values applying to the case of vent conditions based on magma ascent modeling.

It is important to highlight that all these effects were obtained as a result of the complex dispersal process of the eruptive products into the atmosphere without any variation of system parameters or boundary conditions. It is also worth noting that the results obtained are quite reliable with respect to the different assumptions made on vent conditions and clearly indicate a more transient behavior for overpressured conditions of the mixture.

Results predicted by the model suggest that the evolution of quasi-steady explosive eruptions which undergo a transition from a fully buoyant to collapsing behavior, for instance due to a water content decrease of the magma, are characterized by a transitional regime of simultaneous fall-out and emplacement of pyroclastic density currents. This fact may explain the occurrence of interlayered fall-out and flow units observed in many deposits.

Simulation results suggest that a fully convective system would be fed by the entire erupted mass flow-rate of the column and by a grain-size distribution representative of the original mixture. Moving towards the collapsing regime, the convective portion above the fountain would be characterized by a significant decrease in intensity, and therefore in column height, associated with a decrease of the coarse particle content. Eventually, with a total collapse of the column, the plume above the fountain would be strongly reduced and the convective portion of the eruption would be almost exclusively formed by fine ash particles from co-ignimbrite columns. Regarding density currents, simulations indicate that the transition would start with the formation of dilute, low-runout flows and would continue toward denser, longer-runout flows as the mass fraction of collapsing material increased.

Acknowledgements

This work was performed in the ambience of the Volcanic Simulation Group and it was supported by European Community, Project ENV4-CT98-0703, and by Gruppo Nazionale per la Vulcanologia, Istituto Nazionale di Geofisica e Vulcanologia, Italy, Project 2000-2/17. The Istituto CNR-CNUCE is acknowledged for providing computer time. The authors also thank A. Clarke and O. Melnik for the thorough review of the manuscript.

References

Anilkumar, A.V., Sparks, R.S.J., Sturtevant, B., 1993. Geological implications and applications of high-velocity two-phase flow experiments. J. Volcanol. Geotherm. Res. 56, 145–160.

Bacon, C.R., 1983. Eruptive history of Mount Mazama and Crater Lake Caldera, Cascade Range, USA. J. Volcanol. Geotherm. Res. 18, 57–115.

Bertagnini, A., Landi, P., Rosi, M., Vigliargio, A., 1998. The Pomici di Base Plinian eruption of Somma-Vesuvius. J. Volcanol. Geotherm. Res. 83, 219–239.

Bourdier, J.L., Pratomo, I., Thouret, J.C., Boudon, G., Vincent, P.M., 1997. Observations, stratigraphy, and eruptive processes of the 1990 eruption of Kelut volcano, Indonesia. J. Volcanol. Geotherm. Res. 79, 181–203.

Carey, S., Sigurdsson, H., 1987. Temporal variations in column height and magma discharge rate during the 79 A.D. eruption of Vesuvius. Geol. Soc. Am. Bull. 99, 303–314.

Carey, S., Sigurdsson, H., Sparks, R.S.J., 1988. Experimental studies of particle-laden plumes. J. Geophys. Res. 93, 15314–15328.

Carey, S., Sigurdsson, H., Gardner, J.E., Criswell, W., 1990. Variations in column height and magma discharge during the May 18, 1980 eruption of Mount St. Helens. J. Volcanol. Geotherm. Res. 43, 99–112.

Fierstein, J., Hildreth, W., 1992. The Plinian eruptions of 1912 at Novarupta Katmai National Park, Alaska. Bull. Volcanol. 54, 646–684.

Harlow, F.H., Amsden, A.A., 1975. Numerical calculation of multiphase fluid flow. J. Comput. Phys. 17, 19–52.

Hildreth, W., Drake, E.R., 1992. Volcan Quizapu, Chilean Andes. Bull. Volcanol. 54, 93–125.

Neri, A., Dobran, F., 1994. Influence of eruption parameters on the thermofluid dynamics of collapsing volcanic columns. J. Geophys. Res. 99, 11833–11857.

Neri, A., Macedonio, G., 1996. Numerical simulation of collapsing volcanic columns with particles of two sizes. J. Geophys. Res. 101, 8153–8174.

Neri, A., Macedonio, G., Gidaspow, D., Esposti Ongaro, T., 2001. Multiparticle simulation of collapsing volcanic columns and pyroclastic flows. VSG Report 2001-02, ETS, Pisa.

Neri, A., Papale, P., Macedonio, G., 1998. The role of magma composition and water content in explosive eruptions: II. Pyroclastic dispersion dynamics. J. Volcanol. Geotherm. Res. 87, 95–115.

Papale, P., Neri, A., Macedonio, G., 1998. The role of magma composition and water content in explosive eruptions: II. Magma ascent dynamics. J. Volcanol. Geotherm. Res. 87, 75–93.

Rosi, M., Paladio-Melosantos, M.L., Di Muro, A., Leoni, R., Bacolcol, T., 2001. Fall vs. flow activity during the 1991 climactic eruption of Mt. Piñatubo (Philippines). Bull. Volcanol. 62, 549–566.

Sigurdsson, H., Carey, S., 1989. Plinian and co-ignimbrite tephra fall from the 1815 eruption of Tambora volcano. Bull. Volcanol. 51, 243–270.

Sparks, R.S.J., Bursik, M.I., Carey, S.N., Gilbert, J.S., Glaze, L.S., Sigurdsson, H., Woods, A.W., 1997. Volcanic Plumes. J. Wiley and Sons, New York.

Sparks, R.S.J., Francis, P.W., Hamer, R.D., Pankhurst, R.J., O'Callaghan, L.O., Thorpe, R.S., Page, R., 1985. Ignimbrites of the Cerro Galan Caldera, NW Argentina. J. Volcanol. Geotherm. Res. 24, 205–248.

Sparks, R.S.J., Walker, G.P.L., 1977. The significance of vitric-enriched air-fall ashes associated with crystal-enriched ignimbrites. J. Volcanol. Geotherm. Res. 2, 329–341.

Valentine, G.A., Giannetti, B., 1995. Single Pyroclastic beds deposited by simultaneous fallout and surge processes: Roccamonfina Volcano, Italy. J. Volcanol. Geotherm. Res. 64, 129–137.

Valentine, G.A., Wohletz, K.H., 1989. Numerical models of plinian eruption columns and pyroclastic flows. J. Geophys. Res. 94, 1867–1887.

Veitch, G., Woods, A.W., 2000. Particle recycling and oscillations of volcanic eruption columns. J. Geophys. Res. 105, 2829–2842.

Walker, G.P.L., 1981. Plinian eruptions and their products. Bull. Volcanol. 44, 223–240.

Walker, G.P.L., Croasdale, R., 1970. Two plinian-type eruptions in the Azores. J. Geol. Soc. London 127, 17–55.

Wilson, C.J.N., Hildreth, W., 1997. The Bishop Tuff: new insights from eruptive stratigraphy. J. Geol. 105, 407–439.

Wilson, C.J.N., Walker, G.P.L., 1985. The Taupo eruption, New Zealand. I. General aspects. Philos. Trans. R. Soc. London 314.

Wilson, L., Sparks, R.S.J., Walker, G.P.L., 1980. Explosive volcanic eruptions IV. The control of magma properties and conduit geometry on eruption column behavior. Geophys. J. R. Astron. Soc. 63, 117–148.

Wilson, L., Walker, G.P.L., 1987. Explosive volcanic eruptions VI. Ejecta dispersal in Plinian eruptions the control of eruption conditions and atmospheric properties. Geophys. J. R. Astr. Soc. 89, 657–679.

Woods, A.W., 1988. The fluid dynamics and thermodynamics of eruption columns. Bull. Volcanol. 50, 169–193.

Woods, A.W., Bower, S.M., 1995. The decompression of volcanic jets in a crater during explosive volcanic eruptions. Earth Planet. Sci. Lett. 131, 189–205.

Woods, A.W., Caulfield, C.P., 1992. A laboratory study of explosive volcanic eruptions. J. Geophys. Res. 97, 6699–6712.

Woods, A.W., Kienle, J., 1994. The dynamics and thermodynamics of volcanic clouds: theory and observations from the April 15 and April 21, 1990 eruptions of Redoubt Volcano, Alaska. J. Volcanol. Geotherm. Res. 62, 273–299.

Woods, A.W., Wohletz, K.H., 1991. Dimensions and dynamics of co-ignimbrite eruption columns. Nature 350, 225–227.